J. Ocean Univ. China (Oceanic and Coastal Sea Research)
DOI 10.1007/s11802-017-3308-6
ISSN 1672-5182, 2017 16 (6): 1035-1042
http://www.ouc.edu.cn/xbywb/
E-mail:xbywb@ouc.edu.cn

Prediction for Potential Landslide Zones Using Seismic Amplitude in Liwan Gas Field, Northern South China Sea

LI Xishuang[1), 2), *], LIU Baohua[3)], LIU Lejun[1)], ZHENG Jiewen[1)], ZHOU Songwang[4)], and ZHOU Qingjie[1)]

1) *First Institute of Oceanography*, *State Oceanic Administrator*, *Qingdao* 266061, *P. R. China*
2) *Laboratory for Marine Mineral Resources*, *Qingdao National Laboratory for Marine Science and Technology*, *Qingdao* 266071, *P. R. China*
3) *National Deep Sea Center*, *Qingdao* 266237, *P. R. China*
4) *Survey Center of China Oilfield Services Limited*, *Tianjin* 300451, *P. R. China*

(Received September 13, 2016; revised November 1, 2016; accepted December 12, 2016)

Abstract The Liwan (Lw) gas field located in the northern slope of the South China Sea (SCS) is extremely complex for its seafloor topograghy, which is a huge challenge for the safety of subsea facilities. It is economically impractical to obtain parameters for risk assessment of slope stability through a large amount of sampling over the whole field. The linkage between soil shear strength and seabed peak amplitude derived from 2D/3D seismic data is helpful for understanding the regional slope-instability risk. In this paper, the relationships among seabed peak, acoustic impedance and shear strength of shallow soil in the study area were discussed based on statistical analysis results. We obtained a similar relationship to that obtained in other deep-water areas. There is a positive correlation between seabed peak amplitude and acoustic impedance and an exponential relationship between acoustic impedance and shear strength of sediment. The acoustic impedance is the key factor linking the seismic amplitude and shear strength. Infinite slope stability analysis results indicate the areas have a high potential of shallow landslide on slopes exceeding 15° when the thickness of loose sediments exceeds 8 m in the Lw gas field. Our prediction shows that they are mainly located in the heads and walls of submarine canyons.

Key words seismic amplitude; acoustic impedance; shear strength; slope stability analysis; northern South China Sea

1 Introduction

With the advances in exploration and exploitation technologies, oil and gas exploitation has gradually moved towards deep-water areas. However, more risks and challenges are faced in exploitation of deep-water oil and gas (Scheidegger, 1973; Van Eek, 1978; Jeanjean *et al*., 2003; Kvalstad *et al*., 2005), in particular, when the development of deep-water oil and gas field is within a continental slope having complex seafloor (Jeanjean *et al*., 2003; Solheim *et al*., 2005). For the development of deep-water oil and gas field, a challenging problem is the instability of seabed itself, which may result in subsea landslide and turbidity current, damaging basic facilities (Hampton, 1996; Locat and Lee, 2002; Bruschi *et al*., 2006; Zakeri *et al*., 2008, 2009). It is practicable to obtain engineering geological parameters necessary for evaluating the stability of seabed by sampling in shallow water, but it is infeasible to conduct a large amount of sampling or *in situ* testing operations in deep water, owing to technological difficulty and high expense. Critical sampling and careful evaluation are generally carried out only in potential danger zones in deep-water areas.

2D/3D seismic data are generally abundant in the oil and gas fields and seismic attributes derived from seismic data have been extensively used for the characterization of hydrocarbon reservoirs (Rafipour, 1989; Chen and Sidney, 1997; Gastaldi, 2000; Srivastava *et al*., 2004; Sullivan *et al*., 2006; Ahmad and Rowell, 2012; Na'imia *et al*., 2014; Farfour *et al*., 2015). Recently, the use of 3D seismic techniques to image major continental slope morphologies, deposit structures and geohazards has become increasingly common (*e.g.*, Nibbelink and Martinez, 1998; Brand *et al*., 2003; Austin, 2004; Long *et al*., 2004; Bulat and Long, 2005; Mosher, 2006; Gee *et al*., 2006; Bull *et al*., 2009).

Except for seismic acquisition system itself, the main factor influencing seismic amplitude is the reflection coefficient of the interfaces between strata (Sheriff, 1975; Steve, 2004). The relationship between seismic reflection coefficient and acoustic impedance (the product of sediment density ρ and P-wave velocity V) (Sheriff, 1975) can be

* Corresponding author. Tel: 0086-532-88967483
E-mail: lxs@fio.org.cn

expressed as:

$$R = (I_2 - I_1)/(I_2 + I_1) = (\rho_2 \cdot V_2 - \rho_1 \cdot V_1)/(\rho_2 \cdot V_2 + \rho_1 \cdot V_1), \quad (1)$$

where R is seismic reflection coefficient (−1 to +1); I is acoustic impedance, equal to the product of density ρ and velocity V; ρ_1 and ρ_2 are the densities of medium above and under the interface, respectively; and V_1 and V_2 are the P-wave velocities of medium above and under the interface, respectively.

In deep-water area, the sea floor often corresponds to the first strong positive reflection, which is formed due to large differences in the density and velocity between seawater and sediments. As the density and wave velocity of seawater change very little, both seismic amplitude and acoustic impedance of the water body can be regarded as constants. However, large changes in the density and velocity of shallow sediments under seabed make their acoustic impedance fluctuate dramatically. Consequently, for each seismic trace, the peak amplitude of seabed has a close relationship to the acoustic impedance of the shallow sediments under seabed and is influenced comprehensively by the seawater and the sediments within a certain thickness under seabed. The thickness is related to the dominant frequency of seismic records and is approximately half of the dominant wavelength (equal to the velocity/the dominant frequency) (Neidell and Poggiagliolmi, 1977).

Shear strength is a soil mechanical parameter, and an index describing the shear resistance of soil mass (Buchan *et al.*, 1972). Previous research results show that there is a close relation between the shear strength of the subsea shallow soil mass and acoustic impedance (Brand *et al.*, 2003; Arthur Ayres *et al.*, 2013).

The Liwan (Lw) gas field is located in the northern slope of the South China Sea (SCS) with water depth of 200–2500 m and is the first deep-water oil and gas field in China. Previous research results show that a variety of geomorphological units, especially a dozen of small-sized slope-confined canyons, have developed here (Zhu *et al.*, 2010; Zhou *et al.*, 2015; Li *et al.*, 2016), bringing challenge for the gas filed development in this region (Fig.1). The purpose of this paper is 1) to explore the relationships among seismic amplitude, acoustic impedance and the shear strength of subsea shallow sediments in the Lw gas field; and 2) to use the above relationship to predict slope-instability zones. The research results are expected to provide beneficial help for oil and gas field development in the north of the SCS.

2 Data and Methods

2.1 Seabed Peak Amplitude and Water Depth Derived From 3D Seismic Data

Extensive 3D seismic surveys have been conducted in the Lw gas field over the last decade. We derived the seabed peak amplitude and the two-way travel time of the seabed from the seismic data which have a dominant frequency of 65 Hz and a reflection bin of 12.5 m×25 m. In the case of P-wave velocity of shallow sediments taken as V=1600 m s^{-1}, the half of dominant wavelength was 12 m. Therefore the seabed peak amplitude comprehensively reflects the physical properties of sediments within a thickness of 12 m beneath the seabed (Fig.2). Water depths were calculated from the two-way travel time (the sound velocity in seawater was taken as V = 1500 m s^{-1}) and processed into 50 m×50 m grid data (Fig.1b). Further, slope gradients at the same grid interval were obtained.

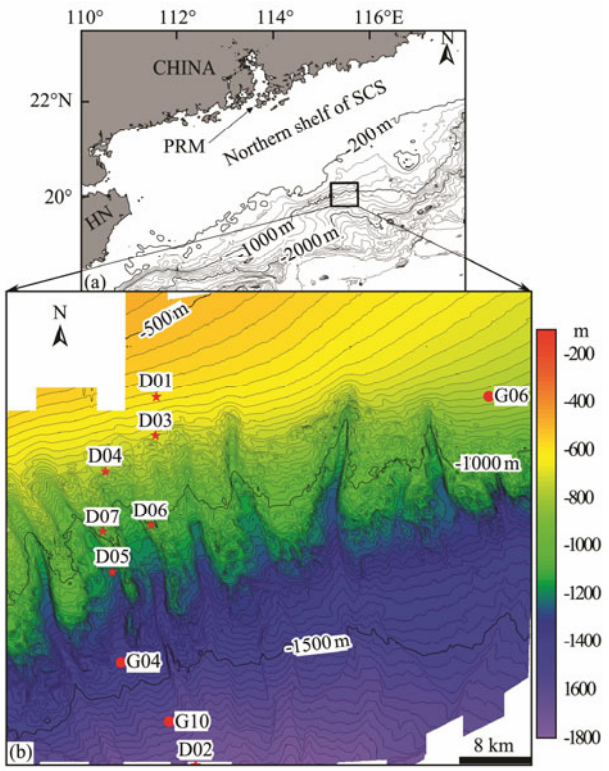

Fig.1 Bathymetric map and the location of sampling stations. (a) Bathymetric map of the north of the South China Sea, plotted based on the USGS 30' data; (b) Bathymetric map of the Liwan gas field based on data derived from 3D seismic data. Red stars denote the boreholes and red dots denote gravity cores. HN, Hainan Island; PRM, Pearl River mouth; SCS, South China Sea.

2.2 Geotechnical Test of Sampled Sediments

7 borehole samples with length of 40 m and 3 gravity

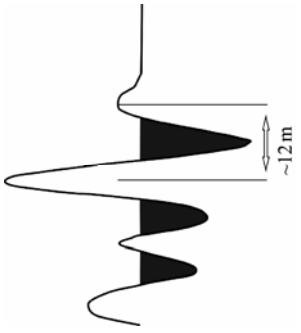

Fig.2 Seabed peak amplitude wavelet (Winggle-trace display). The dominant frequency of seismic data we used is 65 Hz, so that half of dominant wavelength is 12 m for a given P-wave velocity of 1600 m s^{-1} in shallow sediments.

cores over 3 m in length have been obtained in the study area. The sampling stations are shown in Fig.1. The shallow sediments are dominated by silty clay and clay. Laboratory experiments and tests (*e.g.*, natural unit weight (density), P-wave velocity, and undrained shear strength) were conducted. The ring sampler method was used to measure the natural unit weight. The P-wave velocity was measured by using a WSD-3 digital sonic instrument at an interval of 0.5 m, and an acoustic emission frequency of 25 kHz. An electric vane shear tester was used to test the undrained shear strength. The acoustic impedance ($\rho \cdot V$) of the sediments was calculated from natural unit weight and P-wave velocity. Means of these parameters for sediment samples from the uppermost 12 m at all stations are shown in Table 1.

2.3 Methods

In the study, the mathematical statistics method was used for determining the relationships among soil mass shear strength, acoustic impedance and seabed peak amplitude. We employed the limit equilibrium method (Duncan, 1996; Zheng *et al*., 2010), the most common method used to analyze slope stability. An infinite slope model was selected for calculation, in which it was assumed that the fracture plane/slide plane was a plane and the sliding resistance force and sliding force along this surface were regarded as constants. This model is usually applied to slopes with large area and gentle slope gradient, including most subsea slopes (Nixon, 2005). Infinite slope stability is usually indicated by safety coefficient (*Fs*), whose calculation equation is often expressed as follows:

$$Fs = \frac{\text{Sliding resistance force}}{\text{downslide force}} = \frac{(c + (\gamma_w \times z + \gamma \times h) - u)\cos^2 \beta \tan \varphi)}{(h\gamma' \sin \beta \cos \beta)}, \quad (2)$$

Table 1 Geotechnical test data for the uppermost 12 m of cores and the peak amplitude at each station

Station no.	Sediment type	Unit weight (kN m^{-3})	P-wave velocity (m s^{-1})	Acoustic impedance (100 g cm^{-2} s^{-1})	Undrained shear strength (kPa)	Peak amplitude
D01	Silty clay	17.05	1377.0	2395.7	11.80	115493
D02	Silty clay	14.35	1323.6	1938.2	4.70	137348
D03	Silty clay-clay	15.15	1480.3	2288.4	8.15	130320
D04	Silty clay	15.04	1456.8	2235.8	10.94	151185
D05	Silty clay	13.63	1394.3	1939.2	5.09	115207
D06	Silty clay	13.98	1427.6	2036.5	7.05	109153
D07	Silty clay-clay	14.34	1379.2	2018.1	8.03	123957
G04	Silty clay	13.16	1389.4	1865.7	5.17	115594
G06	Silty clay	15.42	1670.7	2628.8	8.24	126094
G10	Silty clay	13.06	1416.7	1888.0	3.38	128216

where c and u are cohesive force and pore pressure, respectively (kPa); γ, γ' and γ_w are the unit weights of saturated soil mass, underwater soil mass, and water, respectively (kN m^{-3}); β and φ are slope gradient, and the internal friction angle of soil mass, respectively (°); z and h are water depth, and sediment thickness, respectively (m). *Fs* is the coefficient of safety, which is a dimensionless index. If $Fs<1$, it indicates that slope failure is more likely to occur; if $Fs>1$, it indicates that the slope is more likely to be stable.

3 Results and Discussion

3.1 Relationships Among Seabed Peak Amplitude, Acoustic Impedance and Shear Strength

Statistical analysis was conducted for the peak amplitudes and the acoustic impedances and a relationship chart was obtained (Fig.3a). The result shows that the seabed peak amplitude increases with the acoustic impedance and indicates a positive correlation between them. This is consistent with the results from Du *et al.* (2014), who derived the relationship between seismic amplitude and impedance using the convolution model and found that there is a positive correlation between seismic amplitude and impedance when seismic wavelet shows a little temporal and spatial variation and the wave impedance of the upper layer also shows small changes. The data points show a relative large scatter, which is possibly because of less sampling stations and inappropriate distribution of core stations. In all the equations expressing the relationship showed in Fig.3a, the linear equation $y_{\text{acoustic impedance}} = 0.0032X_{\text{seismic amplitude}} + 1726$ has the smallest error (the mean difference of acoustic impedance at each core station between measured values and calculated values based on the equation) of less than 11%. It is acceptable in consideration of the large variation of seismic amplitude. The seabed peak amplitude can be converted into acoustic impedance according to the above trend equation (Fig.4).

The relationship between shear strength and acoustic impedance of shallow sediments is obtained by using the same way and the result is shown in Fig.3b. The shear strength increases with the acoustic impedance. Among expressions for the relationship showed in Fig.3b, the exponential equation $y_{\text{shear strength}} = 1\text{E}{-}08X_{\text{acoustic impedance}}^{2.62}$ has the largest correlation coefficient ($R^2 = 0.58$) and the smallest error (the mean difference of shear strength between measured value and calculated value based on the equation) of less than 25%. The acoustic impedance can be converted into shear strength of soil mass according to this trend equation.

Statistical analysis results in different deep-water areas

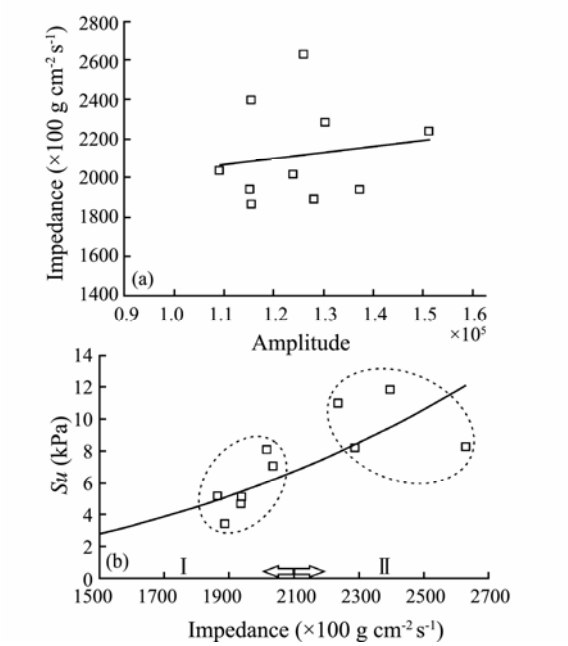

Fig.3 Statistical relationship between seabed peak amplitude and acoustic impedance (a) and the relationship between acoustic impedance and shear strength of shallow sediments (b) *Su* denotes shear strength. All the cores were grouped into two families. The acoustic impedances of family I are less than 2100×100 g cm^{-2} s^{-1}, whereas those of family II are more than 2100×100 g cm^{-2} s^{-1}.

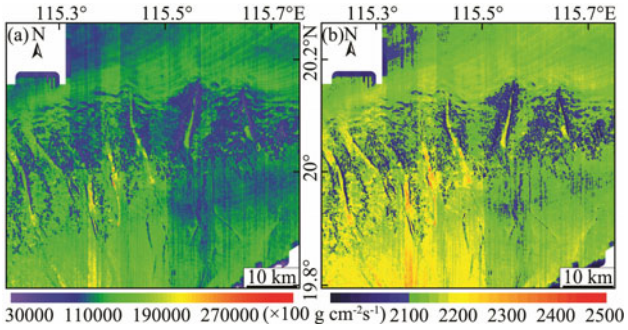

Fig.4 Seabed peak amplitude (a) and calculated acoustic impedance (b) in the Liwan gas field.

(*e.g.*, Brand *et al*. (2003) and Arthur Ayres *et al*. (2013)) show that there is a similar exponential relationship between the shear strength and the acoustic impedance for shallow soils, whereas such relationship is likely affected by the grain size of sediments (Arthur Ayres *et al*., 2013). For fine-grained sediments (*e.g.*, mud or silty mud), the shear strength and the acoustic impedance exhibit an exponential relationship, but for coarse-grained sediments, they exhibit high discreteness. Arthur Ayres *et al*. (2013) speculated that coarse-grained marine soil particles have small contact area, resulting in weak shear strength of soil mass. The dominant sediments in the study area are silty clay and clay and our result continues to confirm the exponential relationship between shear strength and acoustic impedance for fine-grained marine sediments.

The inherent nature of the seabed peak amplitude, the concept of acoustic impedance and their statistical relationship determine a qualitative association between the seabed peak amplitude and the shear strength of shallow soils obtained from cores. The shear strength can be calculated from seabed peak amplitude through the above two statistical equations and a positive relationship between shear strength and seabed peak amplitude can be deduced. The error of calculated shear strength may be big; nevertheless, the variation tendency of shear strength of shallow sediments in the region can be found and the calibrated seabed peak amplitude can be used to guide for further sediment sampling design.

3.2 Classification of Cores by Acoustic Impedance

In order to conduct the slope stability analysis, cores should be classified by the relationship between acoustic impedance and shear strength (Brand *et al*., 2003). The cores with similar acoustic impedance are grouped as one family and slope stability analysis will be carried out for each family. Fig.3b shows that all the cores can be grouped into two families. Six cores in the first family (family I) have mean acoustic impedance less than 2100×100 g cm^{-2} s^{-1} and these cores are G10, G04, D02, D05, D06, and D7. For this family, the change in shear strength with depth is shown in Fig.5a, and the appropriate trend equation to describe the relationship is $y_{\text{shear strength}} = 3.1504 + 0.6526h_{\text{depth}}$ (Fig.6a). Four cores in the second family (family II) have mean acoustic impedance more than 2100×100 g cm^{-2} s^{-1}, ranging from 2200×100 g cm^{-2} s^{-1} to 2700×100 g cm^{-2} s^{-1} and include G06, D01, D03, and D04. For these cores, the change in shear strength with depth of core is shown in Fig.5b, and the appropriate trend equation is $y_{\text{shear strength}} = 5.0023 + 0.9153h_{\text{depth}}$ (Fig.6b).

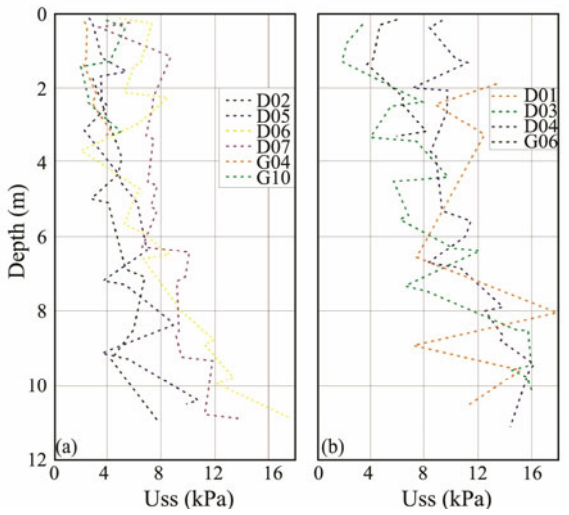

Fig.5 Variation of shear strength with depth for two families. (a) is for family I and (b) is for family II. Uss: undrained shear strength.

The family I with low shear strength corresponds to the area with acoustic impedance less than 2100×100 g cm^{-2} s^{-1}; whereas the family II with high shear strength corresponds to the area with acoustic impedance more than 2100×100 g cm^{-2} s^{-1}.

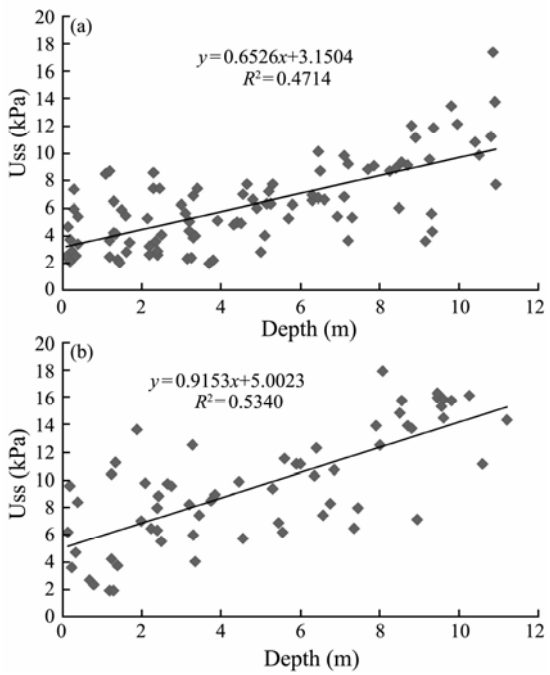

Fig.6 Shear strength *vs.* depth diagrams. (a) is for family I and (b) is for family II. Uss: undrained shear strength.

3.3 Slope Stability Analysis and Results

The slope stability analysis for the subsea shallow soil mass was conducted by using the limit equilibrium method, which is the most common procedure for assessing the risk from instability (Duncan, 1996; Zheng *et al*., 2010). Previous studies show that landslides in the study area were mainly triggered by steepening of the slope due to the erosion of ocean currents or turbidity currents (Qin, 2012; Zhou, 2015). A simple infinite slope model was selected for the analysis and the total stress parameter, undrained shear strength (*Su*), representing short-term water drainage process, was selected for the calculation. When total stress is selected as the parameter, φ=0 and c= *Su* in Eq. (2), and the influences of earthquake action are not taken into account, the slope stability or *Fs* can be simplified into the following:

$$Fs = Su / (\sin(\beta) * \cos(\beta) * \gamma * h) , \quad (3)$$

where *Su* is undrained shear strength (kPa); β is slope gradient (˚); γ is the underwater unit weight of subsea soil (kN m^{-3}); and *h* is the thickness of sediments (m).

Eq. (3) indicates that the slope formed by soil mass with low shear strength has poor stability. Further, it means that the slope with low seabed peak amplitude has poor stability.

3.3.1 *Fs* versus the depth of slide plane at different slope gradients

If the slope gradient (β) is assumed as a constant, we can get the relation curve between *Fs* and the depth (*h*) of slide plane in an area with homogenous shear strength. We calculated safety coefficients for two kinds of slopes with different shear strengths at a series of slope gradients (10˚, 15˚, 20˚, and 25˚) according to Eq. (3). The results are shown in Fig.7 and they indicate the following features:

1) the *Fs* will decrease as the thickness of sediments increases at a given slope gradient if only the gravity of sediment itself is considered; 2) at a given *Fs*, the depth of the slide plane will decrease as the slope gradient increases; 3) at a given slope gradient, as the shear strength decreases, the *Fs* curve will move towards smaller values (*i.e.*, the lower left corner of the coordinate system) and it means that the stable zone (*Fs*>1) will diminish; and 4) for the family I, when the slope gradient is more than 15˚, the critical depth of sediment instability (*Fs* = 1) is 6 m; whereas for the family II, the depth is 9 m.

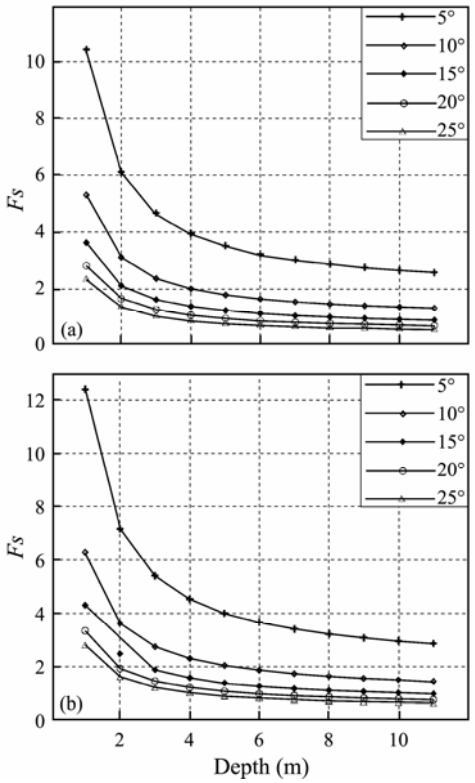

Fig.7 Calculated safety coefficient (*Fs*) *vs.* depth of slide plane at different slope gradients. (a) is for family I and (b) is for family II.

3.3.2 Critical thickness and slope gradient

It is important to know the critical thickness of sediments (*h*) when a specific slope is at the critical state of stability because it can be used to estimate the size of potential landslides (Scheidegger, 1973; Finlay *et al*., 1999; Masson *et al*., 2006). We calculated the range of thickness of sediments with the change of slope gradient at a given shear strengths when *Fs* = 1. The results are shown in Fig.8 and indicate that, for the family I, the critical thickness decreases from 48 m to 2 m as the slope gradient changes from 10˚ to 50˚; whereas for family II, the value decreases from >100 m to 3 m. Comparison of these two families evidently indicates that the critical slope gradient and critical thickness in the family I (shown in Table 2) represent the lower limit of slope stability in the study area. Therefore, potential landslides are more likely to

occur in the area where acoustic impedance is <2100×100 g cm^{-2} s^{-1}, slope gradient is >15˚, and the thickness of loose sediment is >8 m.

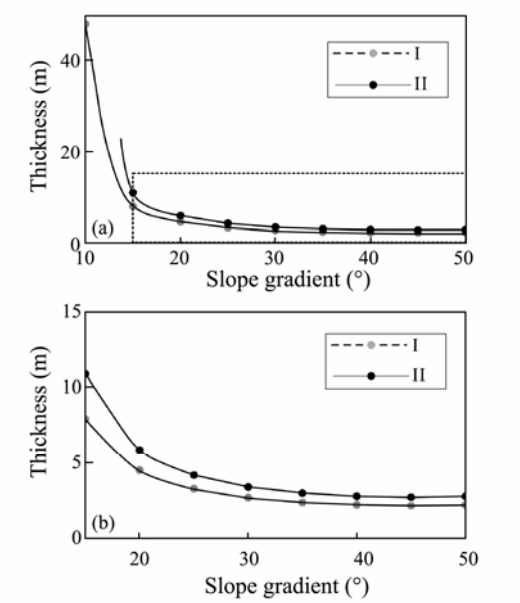

Fig.8 Slope gradient *vs*. thickness of sediments at critical state (*Fs*=1) (a). (b) is the enlargement of dotted line box in (a).

Table 2 Infinite slope stability analysis results

slope gradient (˚)	Critical thickness of sediments (m)
10	48
15	8
20	4.5
25	3.3
30	2.7
>35	2

3.4 Predicting Potential Landslide Zones (PLZs) Based on the Slope Stability Analysis Results

For an area with a given shear strength, when *Fs*=1, the critical slope gradient and the thickness of sediments can be determined by the infinite slope stability analysis results. Sub-bottom profile data reveal that the thickness of shallow loose sediments accumulated on the slope is generally <8 m in the study area. The thicknesses of sediments on slopes less than 15˚ are not as large as the thickness predicted based on the infinite slope stability analyses. Since the slopes are not carrying as much loose sediment as they can, there was no need to investigate flatter slopes. Due to time and budget constraints, it is not necessary to concern the areas where the slope gradient is less than 15˚ in assessing the risk of slope-instability. PLZs can be determined through a multi-layer query of the slope gradient map and acoustic impedance map of the study area. For the family I, the areas where slope gradients are >15˚ were considered as PLZs (pink zones in Fig.9a), whereas for the family II, the areas where slope gradients are >17˚ were considered as PLZs (blue zones in Fig.9a). The results show that most PLZs are located in heads and walls of the canyons where the seafloor often have large slope gradients due to erosion activities of ocean bottom currents, mass movements and turbidity currents (Li *et al*., 2015, 2016).

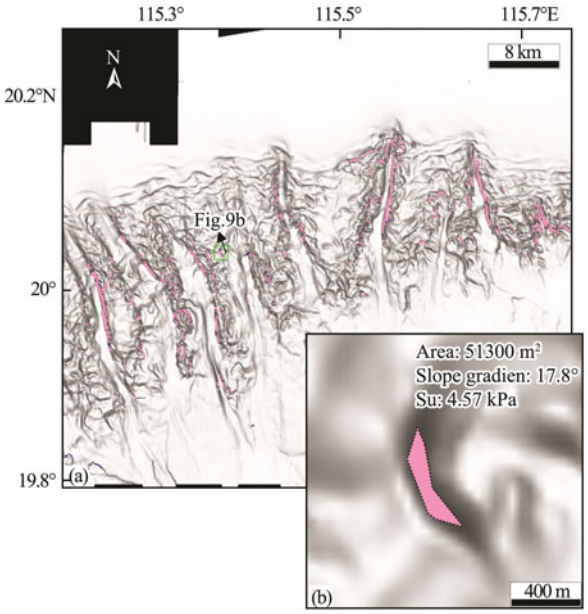

Fig.9 Predicted potential landslide zones (PLZs) (a) and parameters of a PLZ on the slope (b). Pink and blue areas are PLZs for family I and family II, respectively. See (a) for the location of (b).

If a PLZ is selected to be assessed, we can obtain some parameters (*e.g.*, area, slope gradient and mean shear strength) of PLZs. An example of PLZ assessment is shown in Fig.9b. The area of the PLZ in the flank of a canyon is about 51300 m^2, the mean slope gradient is 17.8˚ and the mean shear strength (*Su*) of shallow soil is 4.57 kPa. The area, volume, and strength of sediments for each PLZ are provided as input parameters for further analysis of volume, impact area, run-out and intensity of a potential landslide.

4 Conclusions

In this paper, we have discussed the relationships among seabed peak amplitude, acoustic impedance and shear strength based on 3D seismic data and the geotechnical test data in the Lw gas field, north of the SCS. The statistical results show that the relationships among them are consistent with previous studies although the number of cores are limit and it can be used in the prediction of PLZs. Infinite slope stability analysis indicate that there is high potential of shallow landslide on slopes exceeding 15˚ when the thickness of loose sediments exceeds 8 m in the Lw gas field. Most PLZs are located in heads and walls of the canyons.

Acknowledgements

We would like to thank the technicians for participating in the geotechnical test on sediment cores and thank Dr.

Tongcheng Han and reviewers for their constructive comments. This paper was funded by China National Science and Technology Major Project (No. 2011ZX05 056-001-02).

References

Ahmad, M. N., and Rowell, P., 2012. Application of spectral decomposition and seismic attributes to understand the structure and distribution of sand reservoirs within Tertiary rift basins of the Gulf of Thailand. *The Leading Edge*, **31** (6): 630-634.

Arthur Ayres, N., Joana de Noronha, T. M., Juliana Maria Gonçalves, S., Miguel, R., and Rodrigo, L. B. P., 2013. Geotechnical influence on the acoustic properties of marine sediments of the Santos Basin, Brazil. *Marine Georesources & Geotechnology*, **31** (2): 125-136.

Austin, B., 2004. Integrated use of 3D seismic in field development, engineering and drilling: Examples from the shallow section. In: *3D Seismic Technology: Application to the Exploration of Sedimentary Basin*. Davies, R. J., *et al*., eds., Geological Society, London, Memoirs, 279-296.

Brand, J. R., Lanier, D. L., Berger III, W. J., Kasch, V. R., and Young, A. G., 2003. Relationship between near seafloor seismic amplitude, impedance, and soil shear strength properties and use in prediction of shallow seated slope failure. *Proceedings of the 35th Offshore Technology Conference*. May 5–May 8, Houston, TX, Paper #15161.

Bruschi, R., Bughi, S., Spinazzè, M., Torselletti, E., and Vitali, L., 2006. Impact of debris flows and turbidity currents on seafloor structures. *Norwegian Journal of Geology*, **86**: 317-337.

Buchan, S., McCann, D. M., and Smith, D. T., 1972. Relations between the acoustic and geotechnical properties of marine sediments. *Quarterly Journal of Engineering Geology and Hydrogeology*, **5**: 265-284.

Bulat, J., and Long, D., 2005. Images of debris fans and other deep-sea sediments on the sea bed of the Faroe-Shetland Channel based on 3D seismic data. *Scottish Journal of Geology*, **41** (1): 81-86.

Bull, S., Cartwright, J., and Huuse, M., 2009. A review of kinematic indicator from mass-transport complexes using 3D seismic data. *Marine and Petroleum Geology*, **26**: 1132-1151.

Chen, Q., and Sidney, S., 1997. Seismic attribute technology for reservoir forecasting and monitoring. *Leading Edge*, **16** (5): 445-448.

Du, Q. X., Shen, X. L., Li, D. Q., and Wang, B., 2014. Application of convolution model for prediction of volcanic rocks distribution in Dixi-14 well area in Kelameili gas field, Junggar Basin. *Xinjiang Petroleum Geology*, **35** (3): 282-286 (in Chinese with English abstract).

Duncan, J. M., 1996. State-of-the-art: Limit equilibrium and finite element analysis of slopes. *Journal of Geotechnical Engineering*, **122** (7): 577-596.

Farfour, M., Yoon, W. J., and Kim, J., 2015. Seismic attributes and acoustic impedance inversion in interpretation of complex hydrocarbon reservoirs. *Journal of Applied Geophysics*, **114**: 68-80.

Finlay, P. J., Mostyn, G. R., and Fell, R., 1999. Landslide risk assessment: Prediction of travel distance. *Canadian Geotechnical Journal*, **36** (3): 556-562.

Gastaldi, C., 2000. Reservoir characterizations from seismic attributes: An example from Peciko Field (Indonesia). *AAPG Bulletin*, **84** (9): 1429.

Gee, M., Gawthorpe, R., and Friedmann, S., 2006. Triggering and evolution of a giant landslide, offshore Angola revealed by 3D seismic stratigraphy and geomorphology. *Journal of Sedimentary Research*, **76**: 9-19.

Hampton, M. A., Lee, H. J., and Locat, J., 1996. Submarine landslides. *Reviews of Geophysics*, **34** (1): 33-59.

Jeanjean, P., Hill, A. W., and Taylor, S. L., 2003. The challenges of siting facilities along the Sigsbee escarpment in the southern Green Canyon area, Gulf of Mexico: Framework for integrated studies. *Proceedings of the 35th Offshore Technology Conference*, May 5–May 8, Houston, TX, Paper #15156.

Kvalstad, T. J., Nadim, F., Kaynia, A. M., Mokkelbost, K. H., and Bryn, P., 2005. Soil conditions and slope stability in the Ormen Lange area. *Marine Petroleum Geology*, **22** (1): 299-310.

Li, X. S., Liu, L., Li, J., Gao, S., Zhou, Q., and Su, T., 2015. Mass movements in small canyons in the northeast of Baiyun deepwater area, north of the South China Sea. *Acta Oceanologica Sinica*, **34** (8): 35-42.

Li, X. S., Zhou, Q. J., Su, T. Y., Liu, L. J., Gao, S., and Zhou, S. W., 2016. Slope-confined submarine canyons in the Baiyun deep-water area, northern South China Sea: Variation in their modern morphology. *Mainer Geophysical Research*, **37** (2): 95-112.

Locat, J., and Lee, H. J., 2002. Submarine landslides: Advances and challenges. *Canadian Geotechnical Journal*, **39** (1): 193-212.

Long, D., Bulat, J., and Stoker, M. S., 2004. Sea bed morphology of the Faroe-Shetland Channel derived from 3D seismic datasets. In: *3D Seismic Technology: Application to the Exploration of Sedimentary Basin*. Davies, R. J., *et al*., eds., Geological Society, London, Memoirs, 53-61.

Masson, D. G., Harbitz, C. B., Wynn, R. B., Pedersen, G., and Lovholt, F., 2006. Submarine landslides: Processes, triggers and hazard prediction. *Philosophical Transactions of the Royal Society A*, **364**: 2009-2039.

Mosher, D., 2006. 3D seismic versus multibeam sonar seafloor surface renderings for geohazard assessment. *The Leading Edge*, **25** (12): 1484-1494.

Na'imia, S. R., Shadizadeha, S. R., Riahib, M. A., and Mirzakhanianc, M., 2014. Estimation of reservoir porosity and water saturation based on seismic attributes using support vector regression approach. *Journal of Applied Geophysics*, **107**: 93-101.

Neidell, N. S., and Poggiagliolmi, E., 1977. Stratigraphic modeling and interpretation–Geophysical principals and techniques. *AAPG Special Memoir*, **26**: 389-416.

Nibbelink, K., and Martinez, J., 1998. 3-D seismic coherence, amplitude and bathymetry data definition of Pleistocene to recent sediments along the Sigsbee Escarpment, southeast Green Canyon, Gulf of Mexico, USA. *Transactions, Gulf Coast Association of Geological Societies*, **48**: 289-299.

Nixon, M. F., 2005. Influence of gas hydrates on submarine slope stability. Master thesis. University of Calgary.

Qin, Z. L., 2012. Sedimentary process, distribution and mechanism of mass transport deposits, the slope area of northern South China Sea. PhD thesis. Institute of Oceanology, Chinese Academy of Science (in Chinese).

Rafipour, B. J., 1989. Seismic attributes give clue to reservoir saturation. *World Oil*, **208**: 39-41.

Scheidegger, A. E., 1973. On the prediction of the reach and velocity of catastrophic landslides. *Rock Mechanics*, **5**: 231-236.

Sheriff, R. E., 1975. Factors affecting seismic amplitudes. *Geophysical Prospecting*, **23**: 125-138.

Solheim, A., Bryn, P., Sejrup, H. P., Mienert, J., and Berg, K., 2005. Ormen Lange–An integrated study for the safe development of a deep-water gas field within the Storegga Slide Complex, NE Atlantic continental margin: Executive summary. *Marine Petroleum Geology*, **22** (1-2): 1-9.

Srivastava, A. K., Samanta, B. G., Singh, V., and Sen, G., 2004. Utilization of seismic attributes for reservoir mapping: A case study from the Cambay Basin, India. *First Break*, **22** (4): 31-37.

Steve, H., 2004. Understanding seismic amplitudes. *AAPG Explorer*, **25** (7): 30-31.

Sullivan, C., Nissen, S., and Marfurt, K., 2006. Application of volumetric 3-D seismic attributes to reservoir characterization of karst-modified reservoirs. *GCSSEPM Proceedings*, **26**: 409-428.

Van Eek, W. H., 1978. The challenge of producing oil and gas in deep water. *Philosophical Transactions of the Royal Society of London: Series A*, **290**: 113-124.

Zakeri, A., Høeg, K., and Nadim, F., 2008. Submarine debris flow impact on pipelines–Part I: Experimental investigation. *Coastal Engineering*, **55** (12): 1209-1218.

Zakeri, A., Høeg, K., and Nadim, F., 2009. Submarine debris flow impact on pipelines–Part II: Numerical analysis. *Coastal Engineering*, **56** (1): 1-10.

Zheng, Y. R., Chen, Z. Y., Wang, G. X., and Ling, T. Q., 2010. *Engineering Treatment of Slope & Landslide*. 2nd edition, China Communications Press, Beijing, 94-143 (in Chinese).

Zhou, Q. J., 2015. Identification of submarine landslides and characteristics analysis in the baiyun sag of the south China Sea northern slope. Master thesis. First Institute of Oceanography, SOA (in Chinese).

Zhou, W., Wang, Y., Gao, X., Zhu, W., Xu, Q., Xu, S., Cao, J., and Wu, J., 2015. Architecture, evolution history and controlling factors of the Baiyun submarine canyon system from the middle Miocene to Quaternary in the Pearl River Mouth Basin, northern South China Sea. *Marine Petroleum Geology*, **67**: 389-407.

Zhu, M., Graham, S., Pang, X., and McHargue, T., 2010. Characteristics of migrating submarine canyons from the middle Miocene to present: Implications for paleoceanographic circulation, northern South China Sea. *Marine Petroleum Geology*, **27**: 307-319.

(Edited by Chen Wenwen)